Article

TRANSPARENT PROCESS

THE EMBO JOURNAL

Crystal structure of yeast V_1-ATPase in the autoinhibited state

Rebecca A Oot, Patricia M Kane, Edward A Berry & Stephan Wilkens*

Abstract

Vacuolar ATPases (V-ATPases) are essential proton pumps that acidify the lumen of subcellular organelles in all eukaryotic cells and the extracellular space in some tissues. V-ATPase activity is regulated by a unique mechanism referred to as reversible disassembly, wherein the soluble catalytic sector, V_1, is released from the membrane and its MgATPase activity silenced. The crystal structure of yeast V_1 presented here shows that activity silencing involves a large conformational change of subunit H, with its C-terminal domain rotating ~150° from a position near the membrane in holo V-ATPase to a position at the bottom of V_1 near an open catalytic site. Together with biochemical data, the structure supports a mechanistic model wherein subunit H inhibits ATPase activity by stabilizing an open catalytic site that results in tight binding of inhibitory ADP at another site.

Keywords autoinhibition; reversible disassembly; V_1-ATPase; vacuolar ATPase; X-ray crystallography

Subject Categories Membrane & Intracellular Transport; Structural Biology

DOI 10.15252/embj.201593447 | Received 6 November 2015 | Revised 11 May 2016 | Accepted 12 May 2016 | Published online 13 June 2016

The EMBO Journal (2016) 35: 1694–1706

Introduction

The vacuolar H^+-ATPase (V-ATPase, V_1V_o-ATPase) is a large multisubunit enzyme complex found in the endomembrane system of all eukaryotic cells where it acidifies the lumen of subcellular organelles including lysosomes, endosomes, the Golgi apparatus, and clathrin-coated vesicles (Forgac, 2007). V-ATPase function is essential for pH and ion homeostasis, protein trafficking, endocytosis, MTOR, and NOTCH signaling, as well as hormone secretion and neurotransmitter release. V-ATPase can also be found in the plasma membrane of polarized animal cells where it pumps protons out of the cell, a process required for bone remodeling, urine acidification, and sperm maturation. While complete loss of V-ATPase function in animals is embryonic lethal (Inoue *et al*, 1999), partial loss or hyperactivity of the enzyme has been associated with a wide spectrum of human diseases including osteoporosis (Thudium *et al*, 2012), deafness (Karet *et al*, 1999), renal tubular acidosis (Smith *et al*, 2000), diabetes (Sun-Wada *et al*, 2006), infertility (Brown *et al*, 1997), neurodegeneration (Williamson & Hiesinger, 2010), and cancer (Sennoune *et al*, 2004), making V-ATPase a valuable drug target (Bowman & Bowman, 2005; Fais *et al*, 2007; Kartner & Manolson, 2014).

The V-ATPase couples ATP hydrolysis with the transport of protons across membranes using a rotary mechanism much like the related F- and A/V-type ATPases (Futai *et al*, 2012) (Fig 1A). In the V-ATPase from *S. cerevisiae*, a well-characterized model system for the enzyme from higher organisms, energy coupling requires the concerted action of fourteen different polypeptides that are organized into the ~640-kDa membrane extrinsic V_1-ATPase ($A_3B_3CDE_3FG_3H$) (Kitagawa *et al*, 2008) and the ~330-kDa membrane integral V_o proton channel ($ac_8c'c''de$) (Powell *et al*, 2000; Zhao *et al*, 2015). ATP hydrolysis on the catalytic V_1 is coupled with proton pumping across the V_o via a central rotor made of V_1 and V_o subunits $DFc_8c'c''d$. A peripheral stator complex composed of V_1 subunits E,G,H,C serves to stabilize the motor by binding to the N-terminal cytosolic domain (a_{NT}) of the membrane-anchored a subunit of the V_o (Fig 1B).

As a major consumer of cellular energy, V-ATPase function must be tightly controlled. Regulation of enzyme activity is accomplished by a unique mechanism referred to as reversible dissociation, a condition under which the complex disassembles into cytoplasmic V_1 and membrane-bound V_o (Kane, 1995; Sumner *et al*, 1995). As part of the process, the single-copy subunit C is released from the enzyme and re-incorporated during enzyme reassembly (Kane, 1995). Upon enzyme dissociation, V_1 loses the ability to hydrolyze MgATP (Graf *et al*, 1996; Parra *et al*, 2000) and the V_o no longer conducts protons (Zhang *et al*, 1994), a phenomenon referred to as "activity silencing" (Fig 1C). Reversible dissociation of V-ATPase is well characterized in *S. cerevisiae*, but more recent data suggest that the mammalian enzyme is regulated by a similar process in some cell types. While yeast V-ATPase assembly is governed by environmental conditions such as nutrient availability (Parra & Kane, 1998), salinity, or pH (Diakov & Kane, 2010), the situation in animal cells appears to be more complicated in that next to glucose (Sautin *et al*, 2005), assembly can be triggered by amino acids (Stransky & Forgac, 2015), cell maturation (Trombetta *et al*, 2003), hormones (Voss *et al*, 2007), and growth factors (Xu *et al*, 2012).

An important role in regulating enzymatic activity in V-ATPase is played by the single-copy subunit H, a 54-kDa two-domain

Department of Biochemistry and Molecular Biology, SUNY Upstate Medical University, Syracuse, NY, USA
*Corresponding author. Tel: +1 315 464 8703; E-mail: wilkenss@upstate.edu

polypeptide found at the interface of V_1 and V_o (Wilkens *et al*, 2004). Subunit H plays a dual role in enzyme function: While H is required for ATP hydrolysis and proton pumping in holo V-ATPase (Ho *et al*, 1993), the same subunit functions to inhibit MgATPase activity in membrane-detached yeast V_1, possibly in combination with product inhibition by ADP (Parra *et al*, 2000). The molecular mechanisms by which H functions in silencing MgATPase activity in free V_1 are not well understood, however, largely due to the lack of detailed structural information. Here, we present the crystal structure of the autoinhibited V_1 sector from *S. cerevisiae* (ScV_1) at 6.2–6.5 Å resolution. The structure shows that regulation by reversible dissociation involves a large movement of the C-terminal domain of H (H_{CT}) from its position in V_1V_o to a position at the bottom of the A_3B_3 hexamer in ScV_1. Together with accompanying biochemical data, the structure provides a mechanism of activity silencing in the membrane-detached ScV_1.

Results

Crystallographic investigations of the autoinhibited ScV_1

While subunit C is released into the cytoplasm during reversible enzyme disassembly (Kane, 1995) (Fig 1C), variable but typically substoichiometric levels of C have been seen to co-purify with ScV_1 (Zhang *et al*, 2003; Diab *et al*, 2009; Hildenbrand *et al*, 2010) (see also Fig 5E below). To ensure a homogeneous preparation for crystallogenesis, ScV_1 was therefore purified from a yeast strain deleted for the C subunit (Fig EV1A). Initial crystallization screening identified several conditions that resulted in small needle-shaped crystals. Crystal size and diffraction quality were gradually improved by refining a subset of the initial conditions together with additive screening. Crystals used for collecting initial datasets were obtained in 100 mM HEPES, pH 7.5, 150 mM ammonium sulfate, 12.5 mM magnesium or strontium chloride, and 9.5% PEG 8000 using vapor diffusion or a microfluidic device. A 7 Å resolution dataset collected from one ScV_1 crystal was used to start the structure determination by molecular replacement (MR) (Table 1). Since there is no crystal structure available for the eukaryotic V_1-ATPase, we employed the structure of the nucleotide-free A_3B_3 catalytic hexamer from the *E. hirae* sodium pumping V-type ATPase (EhA_3B_3) (Arai *et al*, 2013) for MR. The primary structures of *E. hirae* and yeast A and B subunits are highly similar (48 and 54% identity, respectively), indicating that the tertiary structures of the bacterial and eukaryotic catalytic subunits are conserved and that the bacterial A_3B_3 catalytic hexamer represents a suitable MR search model for solving the structure of the eukaryotic V_1. The MR with EhA_3B_3 revealed the presence of two ScV_1 sectors in the asymmetric unit (ASU) that were related by twofold non-crystallographic symmetry (NCS) (Appendix Fig S1). The density-modified and NCS-averaged MR map revealed electron density not only for A_3B_3, but also for ScV_1 subunits D,E,G,H that were either

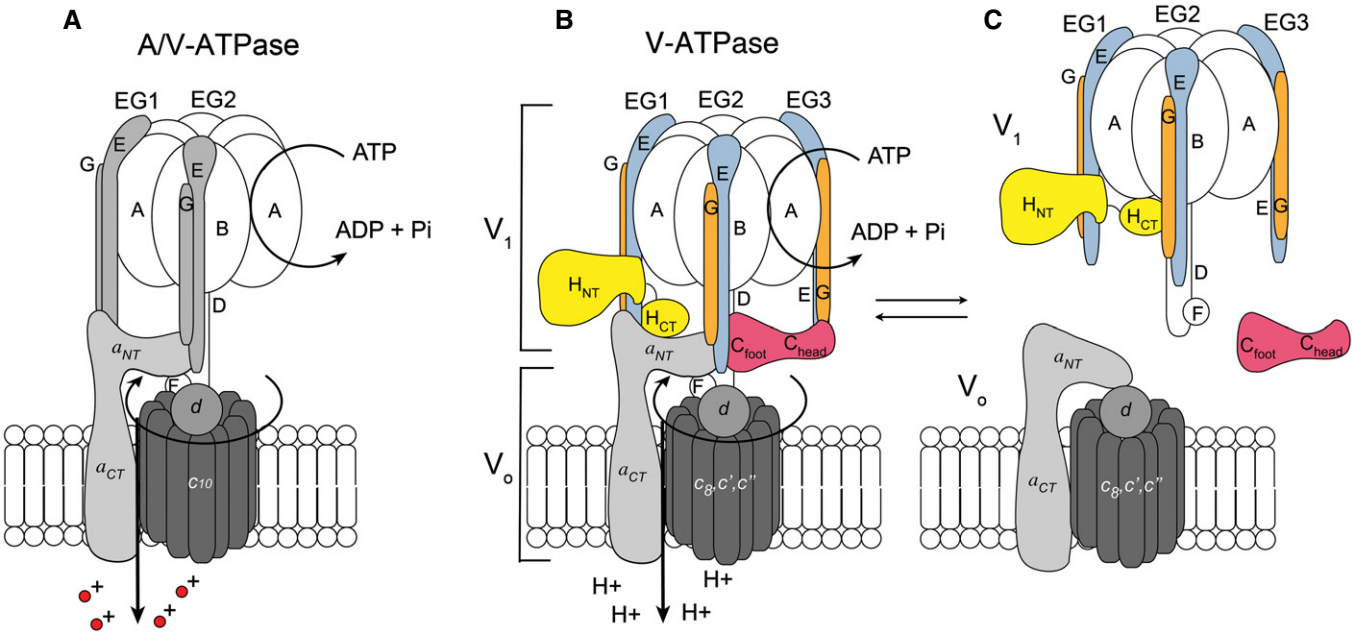

Figure 1. Schematic of the bacterial and eukaryotic V-ATPases.

A Bacterial sodium pumping A/V-type ATPase from *E. hirae* (subunit nomenclature of the eukaryotic V-ATPase). Note that the bacterial A/V-type enzyme has only two peripheral stalks (EG1 and EG2) and no equivalents for the C and H subunits found exclusively in eukaryotic V-ATPase (see next panel).

B Eukaryotic proton pumping V-ATPase. The eukaryotic V-ATPase is a dedicated proton pump composed of a soluble catalytic sector (V_1) and a membrane integral proton translocating sector (V_o). The two functional sectors are linked via a peripheral stator that is formed from the N- terminal extension of the 100-kDa membrane integral subunit (a_{NT}), three peripheral stalks (EG1-3; shown in blue/orange), and subunits C (red) and H (yellow) that are unique to the eukaryotic enzyme.

C Reversible disassembly of eukaryotic V-ATPase. Cellular signals, such as starvation, lead to a dramatic structural rearrangement wherein the V_1 sector dissociates from V_o and subunit C is released from the enzyme. While dissociated, both the V_1-ATPase and V_o proton translocation domain are functionally silenced. This process is fully reversible and upon reassembly, enzymatic activity is restored.

Table 1. Data collection and refinement statistics (molecular replacement).

	ScV_1 Mg	ScV_1 Sr[a]
Data collection		
Space group	C 1 2 1	C 1 2 1
Cell dimensions		
a, b, c (Å)	468.48, 159.74, 245.04	468.02, 159.65, 248.27
α, β, γ (°)	90.00, 113.88, 90.00	90.00, 113.75, 90.00
Resolution (Å)	40.1–7.0 (7.249–7.0)[b]	39.72–6.211 (6.432–6.211)
R_{merge}	0.2558 (2.076)	0.2321 (3.223)
I/σI	7.82 (1.41)	12.01 (0.88)[c]
Completeness (%)	99.0 (94.0)	88.0[d]
Redundancy	8.5 (8.4)	11.1 (11.5)
CC 1/2	0.988 (0.366)	0.983 (0.377)
CC*	0.997 (0.732)	0.996 (0.740)
Refinement		
Resolution (Å)	40.1–7.0	39.72–6.211
No. reflections	26,087	33,464
R_{work}/R_{free}	26.04/30.9	25.45/30.18
No. atoms		
Protein	44,760	47,363
Ligand/ion	0	0
Water	0	0
B-factors		
Protein	291	320
Rms deviations		
Bond lengths (Å)	0.001	0.002
Bond angles (°)	0.42	0.62

[a]Two crystals.
[b]Values in parentheses are for highest resolution shell.
[c]I/σI in the highest resolution shell after elliptical truncation = 1.51.
[d]See Appendix Table S1.

not present in the bacterial complex (E,G,H) or not part of the MR search model (D) (Fig EV1B). Iterative manual placement of available crystal structures for subunits D,E,G, and H followed by refinement allowed for building of a largely complete model of the ScV_1 sector except for subunit F, the base of subunit D and the N-termini of EG2 and EG3 that were not modeled due to insufficient quality of the corresponding electron density. Crystallization conditions were then further refined (8.25% PEG 8000, 250 mM $(NH_4)_2SO_4$, 100 mM HEPES, pH 7.5, 50 mM $SrCl_2$), resulting in slightly larger crystals that diffracted X-rays anisotropically to ~6.2 Å (Table 1). Diffraction data from two crystals were merged and subjected to elliptic truncation with resolution limits of 6.5, 6.2, and 6.7 Å (Appendix Table S1). This higher resolution (hereafter referred to 6.2–6.5 Å) dataset was used in MR employing the 7 Å structure as search model. The resulting electron density was of higher quality compared to the 7 Å data and allowed for modeling of subunit F, the base of subunit D and extension of the N-termini of peripheral stalks EG2 and EG3 (Appendix Table S2). A stereo representation of the final electron density map is shown in Appendix Fig S2. Note that due to the limited resolution of the diffraction data, all polypeptides used for modeling were truncated at the Cβ-position. The more complete model obtained from the 6.2 to 6.5 Å dataset will be discussed in detail below.

Overall structure of ScV_1

The structure presented here represents the highest resolution information available (to our knowledge) for the autoinhibited ScV_1 sector and reveals the conformational changes associated with activity silencing and the loss of binding partners at the membrane. ScV_1 can be divided into an A_3B_3DF catalytic core, three EG heterodimers that serve as peripheral stator stalks (hereafter referred to as peripheral stalks EG1-3) and subunit H, which is unique to the eukaryotic enzyme (Fig 2A). The A_3B_3DF catalytic core is highly conserved between enzymes from prokaryotes to human and contains the catalytic and non-catalytic interfaces between alternating A and B subunits arranged as a hexamer around a central cavity containing the central rotor composed of subunits D and F (see section "Catalytic hexamer and rotary shaft" below). Each of the three peripheral stalks is bound via its C-terminal domain ($E_{CT}G_{CT}$) to the N-terminal β-barrel domain of the corresponding B subunit and crosses a non-catalytic A/B interface on its way toward the base of the hexamer (Fig 2B). However, while the stalks' C-terminal domains are largely invariant, their N-termini ($E_{NT}G_{NT}$) are in different conformations (Fig 2C and D and Appendix Fig S3A). Previously, we have solved the structure of the isolated peripheral stalk heterodimer bound to the C subunit head domain (EGC_{head}, representative of EG3) in two conformations (Oot *et al*, 2012a). In that study, we provided evidence that the EG heterodimers contain two hinges and a partially disordered "bulge" region in subunit G that provide flexibility and that we speculated would play an important role in the mechanism of reversible disassembly (Appendix Fig S3A and B). In peripheral stalks EG1 and EG2, this segment of G is resolved as continuous tubular density, consistent with α-helical structure. In EG3, however, the density is patchy and flattened, indicating presence of the "bulge" structure as seen in isolated EGC_{head} (Fig 2D and Appendix Fig S3C). Peripheral stalk EG3 is bound to the B subunit of a closed A/B pair and its N-terminal domain is bent inwards, wrapping around the C-terminus of the adjacent catalytic A subunit (A_{CT}) (Fig 2D–F and Movie EV1; see also section "Comparison of autoinhibited ScV_1 and ScV_1V_o" below). This suggests that the bulge in subunit G may be present or absent depending upon binding partners and/or nucleotide bound state of the enzyme.

The regulatory H subunit can be seen bound to peripheral stalk EG1 via its N-terminal domain (H_{NT}) while its C-terminus (H_{CT}) is bound at the bottom of the catalytic hexamer near the rotary D subunit (Fig 2A and C). The interactions involving H are of particular interest, as this subunit has been shown to be essential for silencing the ATPase activity of the isolated V_1 sector (see "Subunit H inhibitory interactions" below). While the interactions between the peripheral stalks and a_{NT} and C are lost in isolated V_1, their interactions with the hexamer and the inhibitory subunit H are preserved. The high affinity of the peripheral stalks for the catalytic hexamer and H, combined with the low affinity for the membrane, results in a V_1 sector that can rapidly dissociate from the V_o in response to cellular signals, while keeping its inhibitory subunit bound via one of the peripheral stalks.

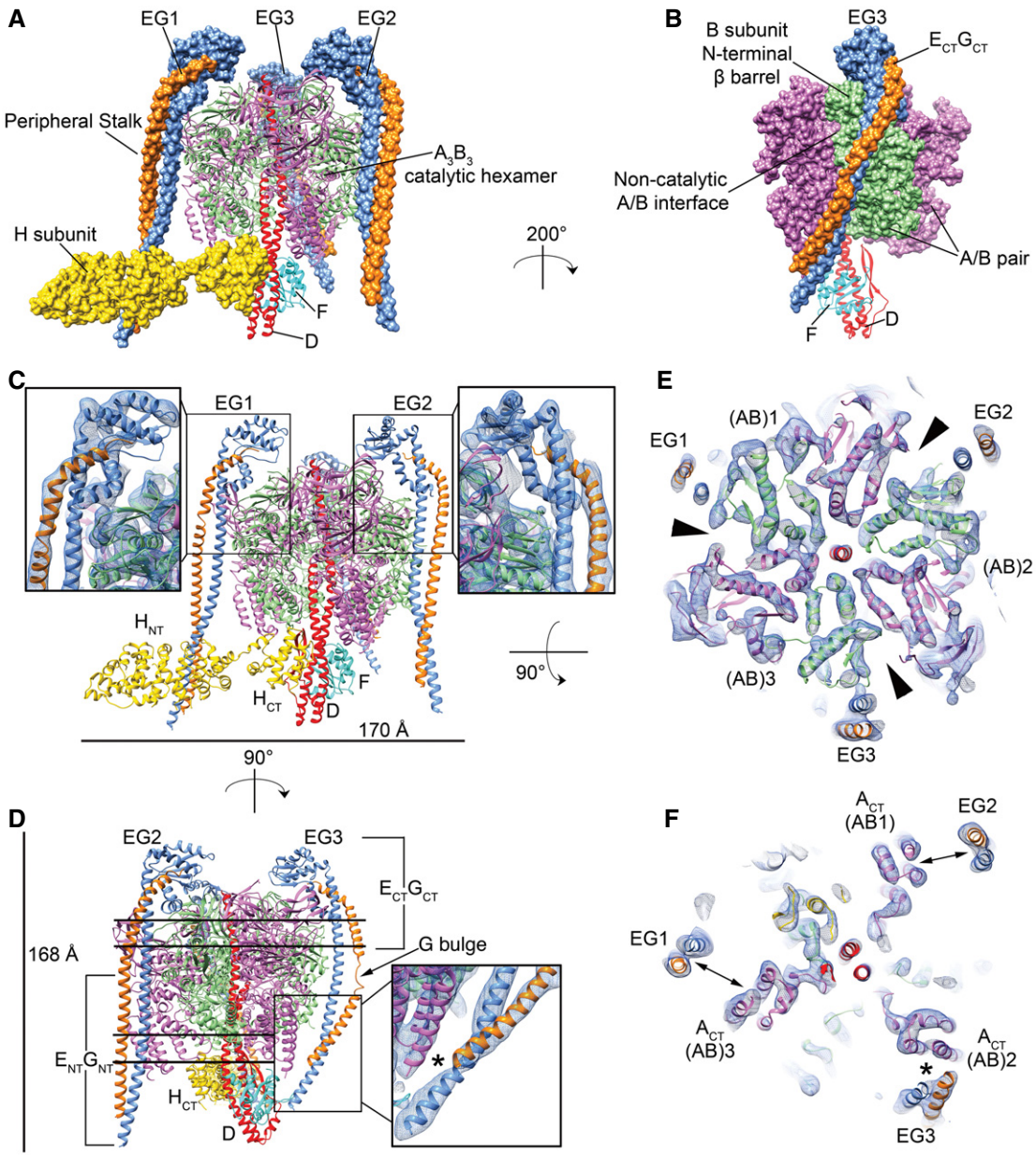

Figure 2. Overall structure of the autoinhibited V_1.

A Structure of autoinhibited ScV_1. The catalytic A (pink) and non-catalytic B (green) subunits are arranged as a heterohexamer around the central rotor subunits D (red) and F (cyan). The three peripheral stalks (EG heterodimers 1–3, blue and orange, respectively) are bound at the periphery of the B subunits. The inhibitory H subunit (yellow) is unique to the eukaryotic V-ATPase. Unless otherwise stated, the coloring scheme used here for the V_1 subunits will be used from here on.

B Interaction of the peripheral stalks with the catalytic hexamer. Each peripheral stalk crosses a non-catalytic A/B interface on its way from the top of the V_1 to the base of the catalytic core. Representative view of the interaction is shown for EG3.

C Interaction of peripheral stalks EG1 and 2 with the catalytic hexamer. The peripheral stalks are bound to the top of the B subunits via their C-termini (boxed). The electron density (contoured at 1.2σ) for the C-terminal domains of EG1 and EG2 is shown in the panels to the left and right.

D The structure of autoinhibited ScV_1 rotated 90° around the vertical from the view shown in panel (A) to highlight peripheral stalks EG2 and EG3. Note the bent appearance of EG3 compared to EG2 along with the presence of a partially unstructured region known as the "bulge" in subunit G (indicated with an arrow). The box shows electron density (contoured at 1.2 σ) for the EG3 N-termini contacting the C-terminal domain of the A subunit of a closed catalytic site (see asterisk). The horizontal lines on the structure indicate the sections shown in panels (E) (upper two lines) and (F) (lower two lines).

E Section through the ScV_1 electron density map showing interaction of the A_3B_3 catalytic hexamer with the peripheral stalks (EG1–3). View is rotated 90° from the view in (A), looking up the central rotor. The A/B pairs forming the three catalytic sites are designated (AB)1-3 according to which of the three peripheral stalks is bound to each B subunit. For example, (AB)1 has peripheral stalk EG1 bound to its B subunit. The black arrowheads indicate the non-catalytic A/B interfaces.

F Section through the ScV_1 electron density map at the level of the N-termini of the peripheral stalks. Note the change in position of the N-termini of the peripheral stalks, which have each crossed a non-catalytic interface (black arrowheads in E) and are now in proximity to the C-termini of the catalytic A subunits (A_{CT}) of the adjacent A/B pairs. While EG1 and EG2 are now near A_{CT} from (AB)3 and (AB)1, respectively (see double headed arrows), only the bent EG3 peripheral stalk is close enough to contact the corresponding A_{CT} from (AB)2 (see asterisk).

Catalytic hexamer and rotary shaft

As mentioned above, the catalytic core (A_3B_3DF) of V-type rotary ATPases is highly conserved, with primary sequence identities between bacterial, yeast, and mammalian A and B subunits of ~50–80%, respectively (Muench *et al*, 2011). Not surprisingly therefore, the structure of the ScV_1 catalytic core is overall very similar to its bacterial counterpart from *E. hirae* (EhV_1) with an rmsd of 2.3 Å. As in EhV_1, the ScV_1 catalytic A and non-catalytic B subunits are arranged as a heterohexamer with their N- and C-termini found distal and proximal to the membrane, respectively (Fig 3A). The N-termini of both subunits are folded in a β-barrel, which together form a contiguous β-structure along the top of the molecule (Fig 3A). Alignment of the A subunits by their N-terminal β-barrels

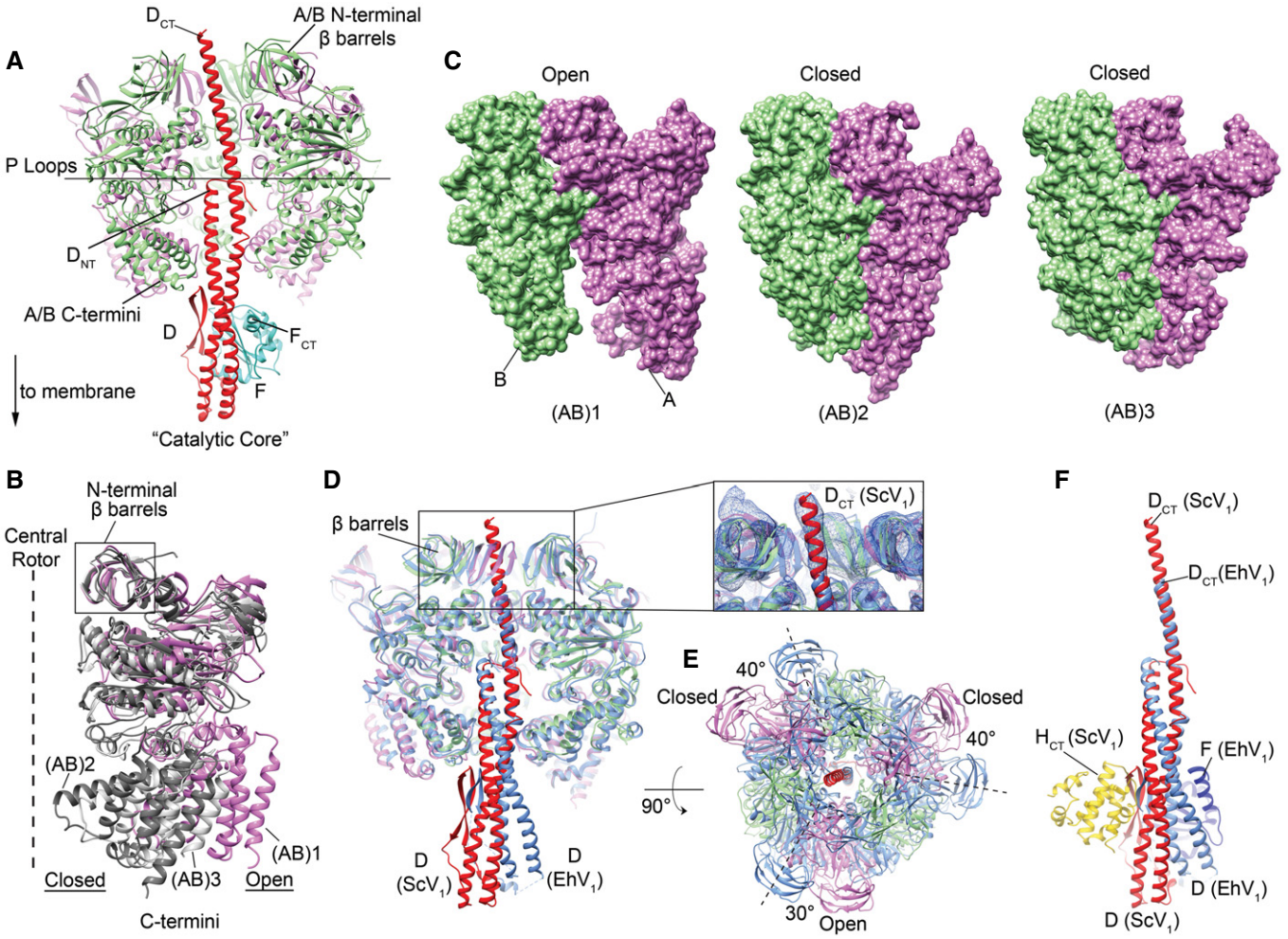

Figure 3. Catalytic A/B pairs and comparison of yeast and bacterial A_3B_3DF.

A The A_3B_3DF complex shown with the subunits unique to the eukaryotic V_1 removed, highlighting the core conserved catalytic complex labeled as "catalytic core". The three peripheral stalks and inhibitory subunit H are found only in the eukaryotic V_1, whereas A_3B_3DF represents the full complement of subunits in the prokaryotic V_1 complex. Notably, the prokaryotic V_1 is an active ATP hydrolase (Arai *et al*, 2009). The orientation of the A and B subunits with respect to the membrane is indicated by the arrow on the left.

B Conformational differences in the catalytic A subunits. The catalytic A subunits are shown aligned by their N-terminal β-barrels, highlighting the change in conformation of C-terminal α-helical bundles associated with the closed ((AB)2 and (AB)3; dark and light gray, respectively) and open ((AB)1; magenta) catalytic sites. Movement of this domain in response to nucleotide occupancy is thought to drive rotation of the central rotor during catalysis.

C ScV_1's catalytic hexamer contains one open and two closed catalytic sites. Side view of the three catalytic hexamer A/B pairs (shown in surface representation). Note that the two closed pairs (AB)2 and 3 are non-equivalently closed.

D Alignment of the A_3B_3DF from ScV_1 and nucleotide-free EhV_1 by the catalytic hexamers. The A_3B_3DF from ScV_1 is shown in the same color scheme as in Fig 2, EhV_1 is in blue. The alignment shows the difference in position of the central rotor subunit, D. Note that the C-terminus of subunit D (D_{CT}) is longer in eukaryotic V-ATPase (see electron density contoured at 1.2 σ in the box to the right).

E ScV_1 and EhV_1 are halted in different rotational positions. Alignment of the A_3B_3DF of ScV_1 and nucleotide-free EhV_1 (blue, with dashed lines drawn through the A subunits) by the central stalk subunit D, reveals that the two catalytic cores are halted in different rotational positions. The autoinhibited ScV_1 requires 40° rotation to overlay its catalytic hexamer with that of the EhV_1.

F Comparison of the D subunits of ScV_1 (red) and nucleotide-free EhV_1 (blue). H_{CT} from ScV_1 is shown in yellow, and subunit F from EhV_1 is shown in dark blue.

illustrates that their C-terminal domains are in different conformations (Fig 3B), consistent with autoinhibited ScV_1 containing one open and two closed catalytic sites as is evident in side views of the three A/B pairs (Fig 3C). From here on, the three catalytic sites will be designated (AB)1-3, depending on which of the peripheral stalks EG1-3 is bound to its B subunit, and following this nomenclature, the open catalytic site is (AB)1 and the two closed ones (AB)2 and (AB)3 (Figs 3C and 2E and F). Note that of the two closed catalytic sites, (AB)2 appears more closed than (AB)3 (Fig 3B and C). The presence of two non-equivalently closed sites has been also observed in the EhV_1 (Arai *et al*, 2013) and in the cryo-EM maps of holo eukaryotic V-ATPase (Zhao *et al*, 2015) (see Discussion section below for more detail).

The central rotor subunit D is an elongated coiled-coil folded as a hairpin, with the N-terminus (D_{NT}) located within and the longer C-terminus (D_{CT}) passing entirely through the A_3B_3 hexamer (Fig 3A). The ~90-Å-long D_{NT} helix penetrates the hexamer up to the level of the phosphate binding or P-loops that are involved in nucleotide binding (Fig 3A). The ~143–Å-long D_{CT} protrudes from the top of the hexamer by ~10 Å, a feature unique to the eukaryotic enzyme (highlighted by the box in Fig 3D). Subunit F is bound to D below the catalytic hexamer via a conserved C-terminal α-helix (F_{CT}; Fig 3A) in a manner similar to the prokaryotic enzyme (Arai *et al*, 2013). While density for the F_{CT} α-helix was observed in both of the ScV_1 structures solved, only the higher resolution structure allowed modeling of the F subunit N-terminal domain, suggesting some flexibility or mobility of the subunit.

Comparing the crystal structures of yeast (ScV_1) and bacterial (EhV_1) catalytic cores reveals considerable differences regarding the position of the D subunit (Fig 3D). Aligning the structure of autoinhibited ScV_1 to available structures of nucleotide-free and AMP-PNP-bound EhV_1 (Arai *et al*, 2013) using the D subunit as reference illustrates that the eukaryotic V_1 is halted in a different rotational position (Fig 3E). The largest angular difference observed (40°) was to nucleotide-free EhV_1, a noteworthy observation as nucleotide-free EhA_3B_3 was used as MR search model to solve the structure of ScV_1. Besides the difference in rotational position of the D subunit in ScV_1 compared to EhV_1, the base of the central rotor is bent in the direction of the interaction between the F_{CT} and a B subunit from the hexamer in *E. hirae*, whereas in ScV_1, the base of the central rotor appears to be more straight and shifted toward the C-terminal domain of the H subunit (Fig 3F). Interestingly, a more straight central rotor is also seen in the ADP-bound catalytic core from the *T. thermophilus* A/V-ATPase (TtV_1; Appendix Fig S4) (Nagamatsu *et al*, 2013), suggesting that the conformation of the DF subcomplex may be influenced by the nucleotide occupancy of the two closed catalytic sites of the complex.

Subunit H inhibitory interactions

Subunit H was the first component of eukaryotic V-ATPase whose structure was solved by X-ray crystallography (Sagermann *et al*, 2001). Subunit H is a two-domain polypeptide with a larger N-terminal domain composed of α-helical HEAT repeats (H_{NT}, residues 1–351) connected to a smaller globular α-helical C-terminal domain (H_{CT}, 356–478) by a flexible linker (Fig 4A). While the NCS-averaged and density-modified MR map showed clear electron density for H_{NT} and H_{CT} (Fig EV1B), the two domains of H had to be modeled separately because of the considerable conformational change required for H_{CT} to assume its inhibitory position in ScV_1 (discussed in "Comparison of autoinhibited ScV_1 and ScV_1V_o" below). The electron density for subunit H is of particularly high quality, showing H_{NT} bound to peripheral stalk EG1 and H_{CT} in contact with the base of the catalytic core (Fig 4A). The interaction between H_{NT} and EG1 is largely mediated by two α-helical segments in H_{NT} (α-14 and α-17, comprising residues 237–255 and 284–296) and a short α-helical stretch in subunit E (residues 26–44) (Fig 4B). The contacts between H_{CT} and the catalytic core are mediated by a loop in H_{CT} (residues 408–414) and two short segments in the C-terminal domain of the B subunit of the open catalytic site (AB)1 (residues around Ile427 and Glu471) together with two α-helical turns in D_{NT} (residues 38–45) (Fig 4C). During catalysis, conformational changes in the catalytic hexamer (Fig 3B and C) drive rotation of the central DF rotor (Movie EV2). As the D subunit forms part of the rotor, the site on D_{NT} for the H_{CT} interaction would only be available for binding in this rotational position (Fig 4D). Further, the site on the B subunit for the H_{CT} interaction is only exposed and available for binding in the open conformation of the (AB)1 pair (Movie EV2). From its inhibitory interactions, it appears that part of the mechanism of H_{CT} inhibition is to stabilize the open conformation of the (AB)1 pair specifically, which would have the additional effect of stabilizing the adjacent closed conformations of the (AB)2 and (AB)3 catalytic sites due to the highly cooperative nature of the catalytic sites in rotary ATPases. As we are able to resolve this interaction in the crystal structure, this must be a specific stopping point associated with inhibition of the enzyme.

Mutational analysis of H_{CT}

The inhibitory interactions between subunit H and the catalytic core are mediated by a loop in H_{CT} (Fig 4C), and surprisingly, while the overall structure and mechanism of eukaryotic V-ATPase, including its unique mode of regulation, are highly conserved, the loop in H_{CT} that is seen in contact with subunits B and D, is not (Fig 5A). To test the possible role of the loop in activity silencing, we performed mutagenesis experiments together with ATPase activity and growth complementation assays. A schematic representation of the mutations is shown in Fig 5B along with a structural alignment of the loop region from autoinhibited V_1 to homology models of the human V-ATPase H subunit (HsH) and the H_{Loop} mutant. While the loop seen in ScH is not present in HsH, it had been shown previously that overexpression of HsH complemented deletion of H in yeast (Lu *et al*, 1998). However, we found that expression in yeast of the two splice variants of HsH (HsH1 and HsH2) from a low-copy plasmid failed to complement the deletion Vma^- phenotype likely due to reduced affinity of HsH for ScV_1 (Fig 5C). In separate experiments, however, recombinant HsH splice variants were able to bind ScV_1 isolated from a yeast strain deleted for subunit H ($ScV_1\Delta H$) in pulldown assays (Appendix Fig S5A and B), but subsequent activity measurements to test whether HsH isoforms inhibit $ScV_1\Delta H$'s MgATPase activity were inconclusive.

Experiments in yeast had shown that while H_{NT} expressed from a plasmid is co-purified with ScV_1, H_{CT} is not (Diab *et al*, 2009), indicating that the majority of the binding energy between ScV_1 and

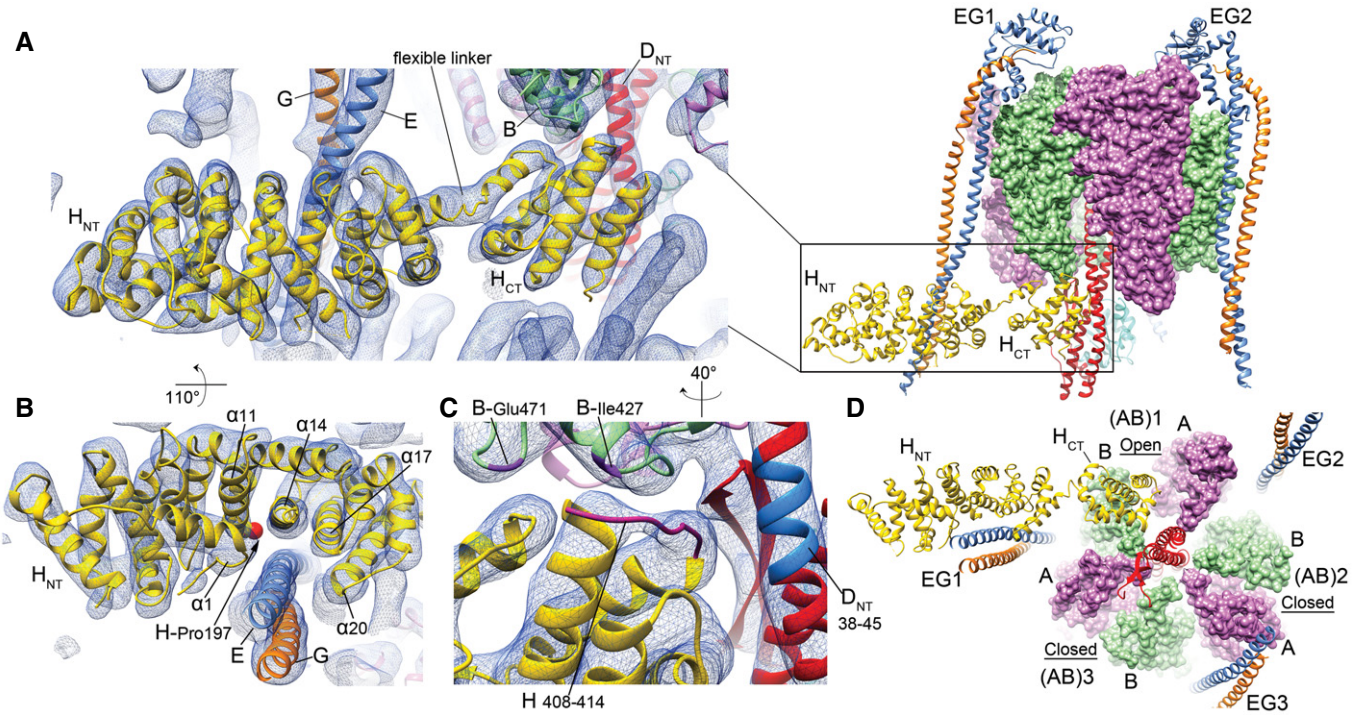

Figure 4. Inhibitory contacts of subunit H.

A ScV_1–H subunit interactions. Region of electron density (contoured at 1.2 σ) outlined by the box in the side view of ScV_1 shown to the right. The H subunit N-terminal domain (H_{NT}) is bound to the N-terminal α-helices of peripheral stalk EG1 while its globular C-terminal domain (H_{CT}) is bound at the base of the catalytic hexamer.

B Interaction between H_{NT} and peripheral stalk EG1. View of H_{NT} as in panel (A) rotated 110° along the horizontal, showing the α-helical HEAT repeats of H_{NT} forming a pocket for binding the N-termini of peripheral stalk EG1. H_{NT}'s α-helices forming the pocket are labeled as in Sagermann *et al* (2001). Pro197 on H_{NT} (red sphere) has been previously shown to cross-link subunit E (Jefferies & Forgac, 2008).

C Interaction between H_{CT} and the base of the catalytic hexamer. The H subunit inhibitory contacts at the base of the ScV_1 are mediated by a loop in H_{CT} (highlighted in magenta) that is seen to contact two short segments of the C-terminal domain of the subunit B from the open catalytic site (AB)1 (highlighted in purple) and two turns of the N-terminal a helix of the central rotor subunit D (highlighted in blue).

D H_{CT} binds to the open (AB)1 pair. View of ScV_1 looking along the central rotor subunit D toward the cytoplasm, showing the position of the H subunit binding at the interface of the open A/B pair (AB)1. The catalytic hexamer is shown in surface representation, and the central rotor, peripheral stalks, and subunit H are shown as ribbons.

H is provided by the interaction between H_{NT} and EG1. We therefore generated a chimeric H subunit construct containing ScH_{NT} and HsH_{CT} (H_{Chim}) to test whether HsH_{CT} can silence MgATPase activity of ScV_1 (Fig 5B). Interestingly, while H_{Chim} complemented the ScH deletion phenotype (Fig 5C), the chimeric subunit failed to silence MgATPase activity in the purified ScV_1 sector (Fig 5D and E). This suggests that the region of H_{CT} that is involved in energy coupling in the holoenzyme is distinct from the portion that functions in activity silencing in isolated V_1.

Sequence comparison between ScH and HsH revealed that while overall identity is only 19%, conservation in the C-terminal domains is significantly higher (30% identity, 52% similarity). Homology modeling of HsH using ScH as a template predicted that the loop seen in contact with B and D subunits in ScV_1 is shorter by three residues and the flanking α-helices are shortened about one turn (Fig 5B, right panel and Appendix Fig S5C). To rule out that regions other than the inhibitory loop are playing a role in activity silencing in ScV_1, the α-helices flanking the loop in ScH were each shortened by one turn (Δ405–408, Δ413–418) to match the local shape of the loop in HsH_{CT} (Fig 5B). While this loop mutant of ScH (ScH_{Loop}) complemented the growth phenotype of the subunit H deletion (Fig 5C), it did not silence MgATPase activity, displaying a specific activity (~9.8 μmol/min/mg) at a level similar to ScV_1ΔH (~12 μmol/min/mg) (Fig 5D). This finding agrees with the results from the chimeric H subunit above and is in line with the H_{CT} loop being important for silencing in ScV_1. In addition, the loop sequence in yeast H_{CT} contains a single aspartic acid residue that is present at an equivalent position in all other organisms analyzed (Fig 5A and B). Mutation of this aspartic residue to an alanine (D410A) complemented the deletion phenotype in yeast (Fig 5C) but had little effect on activity silencing when compared to the wild-type H subunit expressed from a plasmid (Fig 5D). Together, these data indicate that the non-conserved loop is essential for silencing isolated ScV_1, that mutagenesis of the only conserved residue in this region is not sufficient to negate function, and that the dual function of subunit H in activity silencing and energy coupling involves distinct regions in ScH_{CT}.

Comparison of autoinhibited ScV_1 to holo ScV_1V_o

Comparison of the structure of the autoinhibited ScV_1 with the recently reported cryo-EM structures of ScV_1V_o in three different

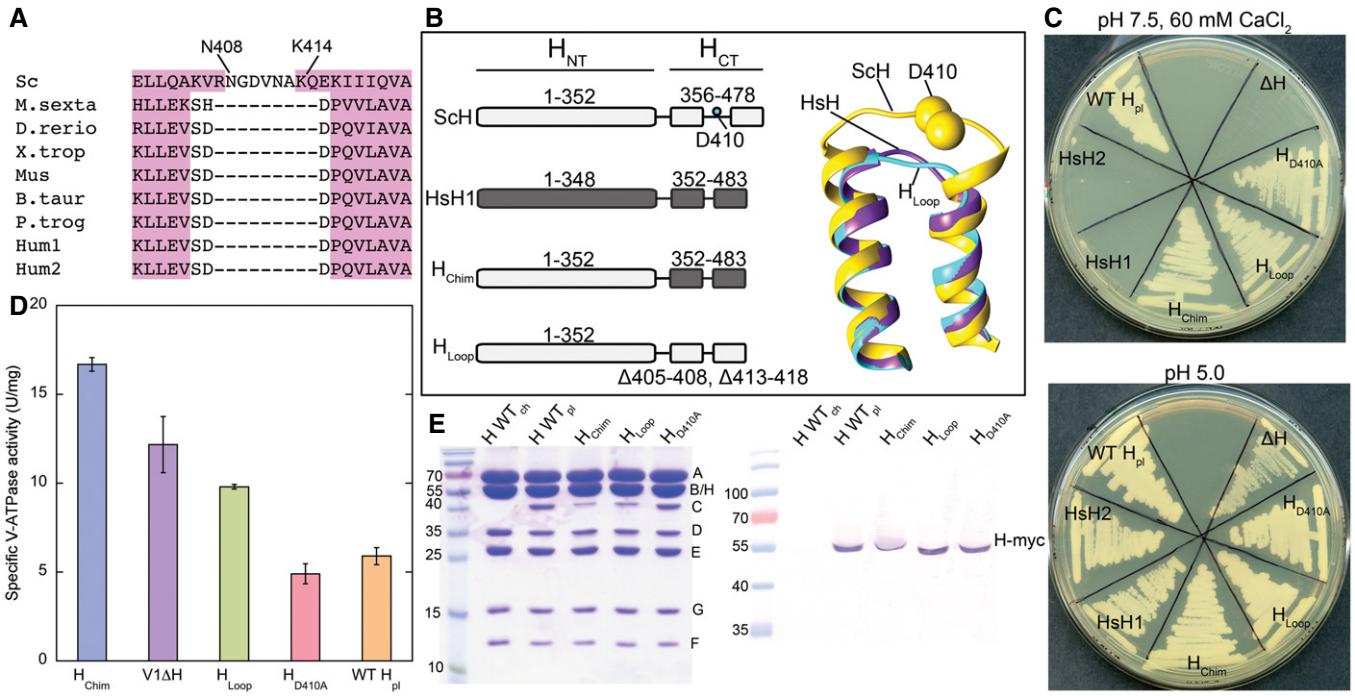

Figure 5. Role of H_{CT} in activity silencing.

A Alignment of the amino acid sequence of the yeast H subunit inhibitory loop region (shown in Fig 4C). The yeast (Sc) loop was aligned with those from insect (*M. sexta*), zebrafish (*D. rerio*), frog (*X. trop*), mouse (*Mus*), bovine (*B. taur*), chimpanzee (*P. trog*), and human (Hum1, Hum2), illustrating the lack of sequence conservation in this region. Pink coloring denotes predicted α-helical secondary structure.

B H subunit mutations. Left panel, schematic representation of the H subunit mutations analyzed. Note that D410 is the only conserved residue in the inhibitory H_{CT} loop. Right panel, overlay of the inhibitory H_{CT} loop from yeast H (yellow) with homology models of the human H (HsH, purple) and yeast H subunit mutant H_{Loop} (cyan).

C Growth phenotype of H subunit mutants. Deletion of V-ATPase subunits from yeast results in a conditional lethal phenotype (Vma^-) characterized by an inability to grow at pH 7.5 in the presence of 60 mM $CaCl_2$ (upper panel), but growth is observed at pH 5 (lower panel). Subunit H mutations were introduced on a plasmid into a yeast strain deleted for the H subunit and their phenotypes assessed. Both human H subunit isoforms (HsH1, HsH2), a chimeric H subunit (H_{Chim}) containing ScH_{NT} and HsH_{CT}, mutations in yeast intended to mimic the length of the human H loop sequence and accessibility (H_{loop}), and a point mutation of the conserved aspartic acid residue in the loop sequence (H_{D410A}) are shown compared to the H subunit deletion (ΔH) and wild-type H on a plasmid (H WT_{pl}). All grow on pH 5 medium, but the human isoforms failed to complement the deletion phenotype.

D ATPase activity of H subunit mutants. The ScV_1 sectors were purified from each strain that complemented the phenotype as well as from ScV_1ΔH, for comparison of MgATPase activity. Average specific activities are shown plotted ± s.e.m. from two independent purifications. The ScV_1 sector containing chromosomally encoded H subunit shows no detectable MgATPase activity (Parra *et al*, 2000; Zhang *et al*, 2003), whereas ScV_1 containing plasmid-borne wild-type H (H WT_{pl}) exhibits low levels of activity likely due to reduced expression from the low-copy plasmid. The H_{Chim} and H_{Loop} mutants lead to a loss of activity silencing, displaying nearly the same activity as ScV_1ΔH.

E SDS–PAGE and Western blot analysis of ScV_1 preparations. Left panel, 15% SDS–PAGE of ScV_1 purified from the subunit H mutant and WT strains. Note that H WT_{ch} is purified from a yeast strain deleted for the C subunit (used for crystallization). The remaining strains contain subunit C, which is co-purified with ScV_1 in varying levels. Note that while H WT_{ch} ScV_1, which is expressed from a strain deleted for subunit C, displays no detectable MgATPase activity, the H subunit mutants co-purified with the most C subunit display the least activity, suggesting that absence or presence of subunit C has no effect on MgATPase activity. Right panel, immunoblot probed with an antibody directed against the N-terminal Myc-tagged mutant H subunits expressed from a plasmid. Note that the levels of mutant H expression do not appear to vary from strain to strain.

states (Zhao *et al*, 2015) revealed that autoinhibited ScV_1 most closely matches the conformation of the ATPase sector of the "state 2" conformation (Appendix Table S3). However, alignment of the two structures revealed significant conformational differences in all the V_1 subunits except the A_3B_3 hexamer (Fig 6 and Movie EV3). While the C-terminal domains of the peripheral stalks are largely invariant, their N-terminal domains are in different conformations in ScV_1 and ScV_1V_o (Fig 6A–D), in line with their loss of binding partners upon enzyme disassembly (a_{NT} for EG1 and EG2 and subunit C for EG2 and EG3). In ScV_1, H_{NT} and the N-terminal domain of EG1 move outwards toward the periphery of the V_1 (Fig 6A and B, and Movie EV3). In addition, a striking change is seen in peripheral stalk EG3 that is bound to the C subunit in the assembled enzyme but binds to the C-terminal domain of an A subunit of closed catalytic site (AB)2 in ScV_1 (Fig 6C and D; see also Fig 2D–F).

The most dramatic change is seen in the position of H_{CT}, rotating ~150° from a position in V_1V_o where its C-terminal α-helix is in contact with a_{NT} to its position at the bottom of the catalytic hexamer in free ScV_1 as described above (Fig 6C and E). Interestingly, this change in H_{CT} conformation is accompanied by a repositioning of subunit D to accommodate H_{CT} (Fig 6E). The apparent flexibility of H_{CT} can be further illustrated upon comparison of the available structure of the isolated H subunit to that in

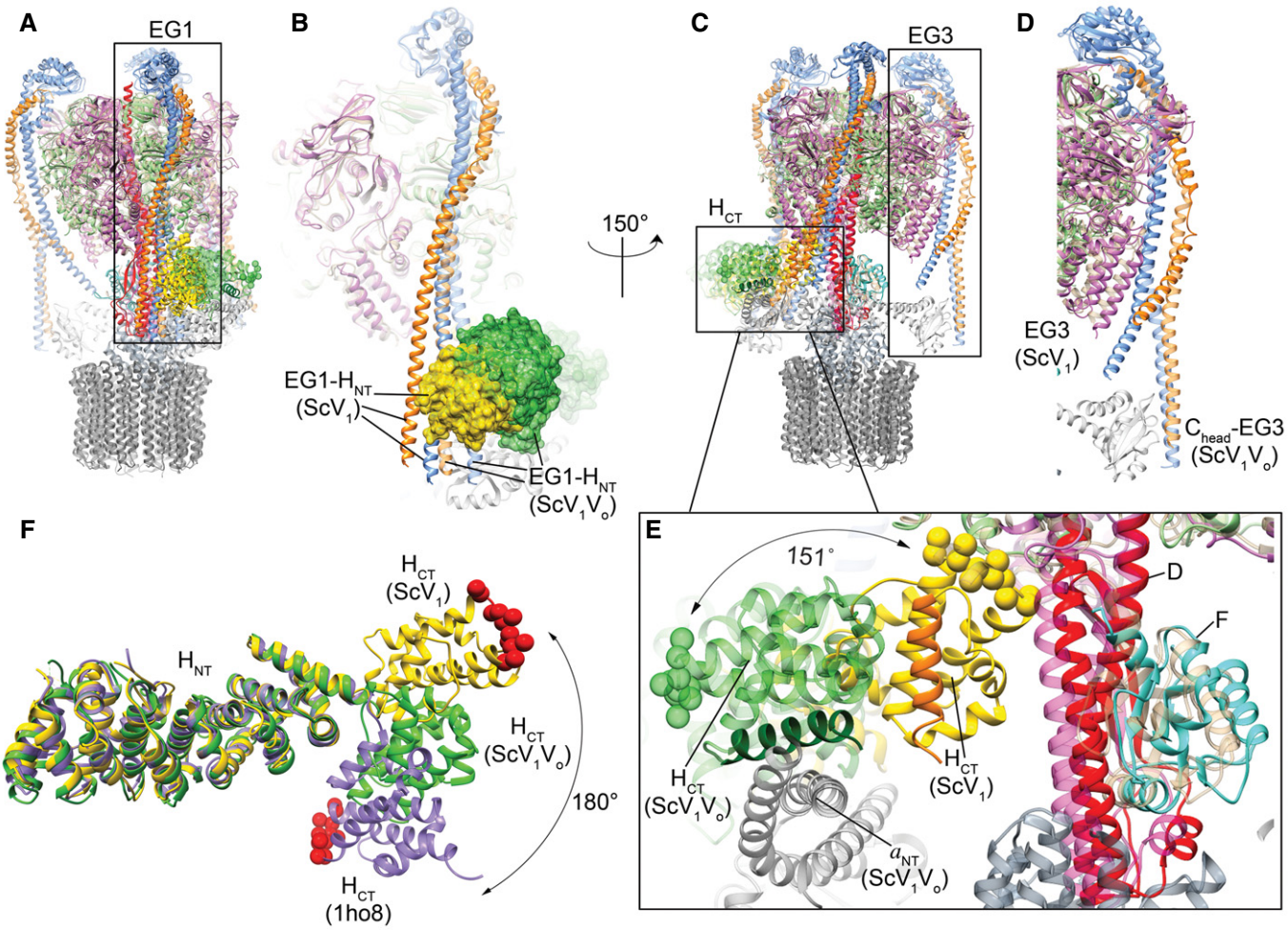

Figure 6. Comparison of ScV_1 to the assembled ScV_1V_o holoenzyme.

A Overlay of ScV_1 and the cryo-EM structure of the V_1V_o holoenzyme in "state 2" (Zhao *et al*, 2015). The structures of ScV_1 and ScV_1V_o were overlaid by aligning the A_3B_3 catalytic hexamers, thus highlighting structural differences in the central rotor and peripheral stator subunits. Coloring of ScV_1V_o (shown as semi-transparent ribbons) is as used throughout for ScV_1 for all but the A_3B_3F (tan), subunit H (dark green), subunit C, and V_o domain (gray). The EG1–H_{NT} interaction is boxed. Note the shift in position of H_{NT} and EG1 between ScV_1 and ScV_1V_o.

B Comparison of peripheral stalk EG1 and H_{NT} in ScV_1 versus ScV_1V_o. The boxed view in (A) is shown enlarged. The N-terminal α-helices of peripheral stalk EG1 and H_{NT} change in conformation, likely induced by the movement of H_{CT} when going from the holoenzyme to the autoinhibited conformation.

C View as in (A) rotated 150° around the vertical. Comparisons of peripheral stalk EG3 and H_{CT} are boxed.

D Comparison of peripheral stalk EG3 in ScV_1 versus ScV_1V_o. In ScV_1V_o, EG3 binds to the C subunit head domain (C_{head}; gray) whereas in ScV_1, EG3 is bent toward the C-terminal domain of a catalytic A subunit (enlarged view of box-labeled EG3 in panel C).

E Comparison of H_{CT}'s conformation in ScV_1 versus ScV_1V_o. Enlarged view of box-labeled H_{CT} in panel (C) highlighting the conformational changes and binding interactions of H_{CT}; for clarity only a_{NT}, H_{CT} and the central rotor (DF) are shown. In ScV_1V_o, the most C-terminal α-helix (dark green) of H_{CT} (green) binds to a_{NT} (light gray), with the inhibitory loop (green spheres) rotated away and inaccessible for binding the B subunit and the central stalk (transparent red). In ScV_1, the H_{CT} (yellow) inhibitory loop (yellow spheres) binds to the central stalk subunit D (red) and the B subunit of the open (AB)1 catalytic site. The difference in conformation between ScV_1V_o and ScV_1 involves a ~150° rotation of H_{CT}. Note that the H_{CT} loop (spheres) is rotated away from the central stalk in ScV_1V_o whereas in ScV_1, the C-terminal α-helix (orange) involved in binding a_{NT} is rotated away and unavailable for rebinding to the membrane.

F H_{CT} conformational changes. Available subunit H structures as obtained for isolated H (Sagermann *et al*, 2001) (purple), in ScV_1V_o (Zhao *et al*, 2015) (green) and in ScV_1 (yellow) are shown aligned by their N-terminal domains (H_{NT}) illustrating the conformational flexibility of H_{CT}. The loop involved in inhibition of ScV_1 is shown as red spheres, highlighting the 180° rotation of H_{CT} when going from the conformation of isolated H (H_{CT} 1ho8) to the inhibitory conformation in ScV_1 (H_{CT} ScV_1).

ScV_1V_o and in ScV_1 (Fig 6F). Based on this comparison, H_{CT} undergoes a 180° rotation from its position in isolated H to that in the autoinhibitory conformation in ScV_1. The alignment further suggests that H_{CT} can adopt multiple low-energy conformations and that its flexibility is required for the inhibitory function in ScV_1 and for coupling ATP hydrolysis with proton transport in ScV_1V_o.

Discussion

Activity silencing in ScV_1

Previous studies have shown that subunit H, specifically H_{CT}, is essential for both inhibition of MgATPase activity in free ScV_1 (Parra *et al*, 2000; Diab *et al*, 2009) and efficient coupling of ATP

hydrolysis with proton pumping in holo ScV_1V_o (Ho *et al*, 1993; Liu *et al*, 2005; Flannery & Stevens, 2008). Exactly how H_{CT} performs these dual functions, however, was not understood. In EM reconstructions of holo V-ATPase (Zhang *et al*, 2008; Zhao *et al*, 2015), H_{CT} is seen in contact with a_{NT} whereas in the crystal structure of membrane-detached ScV_1 presented here, H_{CT} binds (and thereby links) the B subunit of the open catalytic site and the central rotor subunit D. Remarkably, to transition from its activating position in ScV_1V_o to its inhibitory position in ScV_1, H_{CT} must undergo a ~150° rotation around the linker connecting H_{CT} and H_{NT} (Movie EV2). It has been shown that when the flexibility of the linker is impaired, subunit H's ability to inhibit MgATPase activity of $ScV_1\Delta H$ is significantly reduced (Benlekbir *et al*, 2012), indicating that H_{CT}'s interaction at the bottom of V_1 is indeed responsible for activity silencing. Photochemical cross-linking on the other hand suggested that activity silencing maybe due to a direct interaction of H_{CT} with the rotor subunit F (Jefferies & Forgac, 2008); however, for reasons that are unclear, this interaction is not observed in the structure of autoinhibited ScV_1 presented here.

From kinetic profiles of Mg or CaATPase activity assays of $ScV_1\Delta H$ or ScV_1, respectively, it has been proposed that ADP inhibition may contribute to activity silencing independent of subunit H (Parra *et al*, 2000). Interestingly, while ScV_1 purified using ammonium sulfate precipitation and ion exchange chromatography contained no bound nucleotide (Parra *et al*, 2000), the ScV_1 as purified here by affinity chromatography contains ~1.3 mol/mol ADP. $ScV_1\Delta H$ on the other hand retained only ~0.4 mol/mol of the nucleotide, indicating that subunit H, by stabilizing an open catalytic site near EG1, leads to increased affinity for inhibitory ADP at another site, which in turn results in activity silencing. Since there are two non-equivalently closed catalytic sites in ScV_1 (Fig 3B and C), it is likely that one of these sites is completely filled and the other partially occupied with nucleotide. The presence of strong positive difference density near the P-loop in (AB)2 indicates that the inhibitory nucleotide is bound in the closed catalytic site near EG2 and while we cannot assign the identity of the nucleotide at this resolution, our biochemical measurements indicate that it is likely to be ADP (Appendix Fig S6). Remarkably, the N-terminal domain of EG3 is seen to wrap around the C-terminal domain of the A subunit of (AB)2 and it is possible that this interaction, seen only in membrane-detached V_1, provides yet another mechanism to stabilize the closed conformation of (AB)2 for efficient trapping of inhibitory ADP. Taken together, the data suggest that activity silencing is not caused by a single high-affinity protein–protein interaction, but is rather the result of several interactions, which must be readily reversible to allow for efficient enzyme reassembly. Interestingly, inhibition of ScV_1 by ScH appears to be mediated by a loop in H_{CT} that is not conserved in other species, and while a chimera of yeast H_{NT} and human H_{CT} is able to complement the Vma^- phenotype of a subunit H deletion, the human H_{CT} does not function in silencing ScV_1's MgATPase activity. Whether mammalian subunit H plays a role in activity silencing similar to yeast H remains to be determined.

Comparison of ScV_1 and ScV_1V_o and implications for the mechanism of reversible dissociation

Previous studies have shown that enzyme activity is required for regulated dissociation but not for reassembly or V-ATPase biogenesis (Parra & Kane, 1998). As this has been shown to be the case even in enzymes that can bind nucleotide, but not hydrolyze it, it has been proposed that the V-ATPase must adopt a specific conformation during rotary catalysis that favors enzyme dissociation (Muench *et al*, 2011). A comparison with the recent cryo-EM structures of ScV_1V_o (Zhao *et al*, 2015) showed that autoinhibited ScV_1 resembles the V_1 conformation of state 2 (Appendix Table S3) with its open catalytic site and D_{NT} near EG1 and H_{CT}. State 2 must therefore represent the conformation where V_1 can dissociate from V_o. The comparison also reveals the distinct binding sites on H_{CT} for a_{NT} (in ScV_1V_o) and B/D_{NT} (in ScV_1), each mediating, as mentioned above, a different function: energy coupling in ScV_1V_o and silencing in ScV_1, consistent with the biochemical assays presented here involving chimeric and loop mutant H subunits. Besides the different and opposing function mediated by each of these two distinct binding sites on H_{CT}, they appear also to prevent both re-binding of V_1 to V_o when dissociation is favored and prohibit inhibitory interactions from forming when turnover and assembly is required (Movie EV3). For example, it has been shown that ScV_1 does not bind a_{NT} *in vitro* (Diab *et al*, 2009), a result that can be explained by the fact that the most C-terminal α-helix on H_{CT} that binds a_{NT} in V_1V_o is hidden in V_1 due to the 150° rotation of H_{CT} during disassembly. Unintended reassembly may also be prevented by the conformational change of peripheral stalk EG3 that occurs as a result of enzyme disassembly. EG3 is bound to C_{head} in ScV_1V_o, but as subunit C is released into the cytoplasm upon V-ATPase dissociation, the bent conformation of EG3 seen in ScV_1 may help to prevent rebinding of C, which is required for functional association of V_1 with V_o. Indeed, V_1 purified from yeast cytoplasm or insect midgut has variable levels of C subunit bound, ranging from non-detectable (Graf *et al*, 1996; Parra *et al*, 2000) to more significant amounts (Zhang *et al*, 2003; Diab *et al*, 2009; Hildenbrand *et al*, 2010), consistent with EG3 adopting a conformation unfavorable for C_{head} binding. Together, the differences in conformations of ScV_1 versus ScV_1V_o not only allow silencing of ScV_1's MgATPase activity but may also serve to prevent functional re-association of V_1 to V_o when the disassembled state is required.

The structure presented here of ScV_1 along with the available structures of V_1V_o and biochemical data allow for a more detailed picture of the mechanism of regulation by reversible dissociation. In holo V_1V_o, a_{NT} serves as membrane anchor for V_1 subunits EG1, H_{CT}, EG2, and C_{foot}. We have previously shown that the ternary a_{NT}-EG2-C_{foot} junction is formed by low-affinity interactions and we proposed that targeting of one of these interactions by an as yet unknown process would initiate enzyme disassembly (Oot & Wilkens, 2012b). Recently, our laboratory has shown that enzyme dissociation involves a large movement of a_{NT} from its position near EG2 and C_{foot} in V_1V_o to a position near subunit d in free V_o (Couoh-Cardel *et al*, 2015). We speculate that once the signal is received targeting the low-affinity a_{NT}-EG2-C_{foot} junction, a_{NT} changes conformation to bind subunit d, thereby breaking the interaction with H and allowing H_{CT} to rotate 150° to bind to and stabilize the open (AB)1 pair found in state 2 of ScV_1V_o (Movie EV4). As the dissociation signal may present itself to the enzyme in any of the three (or more) catalytic states of the enzyme, it seems likely that once state 2 is reached, the conformational

changes associated with V_1V_o dissociation and silencing of free V_1 and V_o are more favorable than maintaining the holoenzyme. The above-mentioned requirement for ATP hydrolysis in dissociation may serve multiple purposes: (i) achieving state 2 in which (AB)1 and D_{NT} are in proximity to subunit H, (ii) generating the torque needed to break remaining interactions with the membrane sector, and (iii) leaving inhibitory MgADP in catalytic site (AB)2. The model of enzyme regulation proposed here thus couples the dissociation event with activity silencing directly. As regulated disassembly is fully reversible, the enzyme must come together again in a rapid and efficient manner when its function is required. While still unresolved, the pathways involving re-association have been shown to be distinct from those involved in dissociation. The dramatic conformational changes in ScV_1 and V_o subunits as a result of enzyme dissociation may explain the reported inefficiency of direct rebinding of ScV_1 to the membrane *in vitro*, requiring extreme conditions such as low pH (Parra & Kane, 1996), and may account for the requirement of a dedicated chaperone known as the RAVE complex (Seol *et al*, 2001; Smardon *et al*, 2002) for reassembly *in vivo*. The exact function of the RAVE complex is currently unknown, but there is evidence that the chaperone displays several distinct binding sites for subunits C, EG, and a_{NT} (Smardon *et al*, 2015), a subset of the very same subunits that change conformation during regulated enzyme disassembly as described above.

In conclusion, eukaryotic V-ATPase is a dynamic molecular machine. The structural model of ScV_1 presented here highlights the structural changes occurring in the V_1-ATPase sector as a result of activity silencing and reversible disassembly. Aberrant V-ATPase activity has been recognized as being responsible for, or associated with many devastating human conditions. Activity silencing and the mechanism of reversible dissociation may thus offer a way to modulate enzyme activity by, for example, the design of molecules that either promote or inhibit the process. These kinds of studies would benefit from higher resolution information, efforts that are ongoing in our laboratory.

Materials and Methods

Protein purification

ScV_1 used for crystallization was affinity purified from a yeast strain deleted for the genes encoding subunits C (VMA5) and G (VMA10) (vma5Δ::Nat, vma10Δ::URA3) and transformed with a pRS315 vector containing N-terminally FLAG tagged G subunit (Zhang *et al*, 2003). $ScV_1\Delta H$ and ScV_1 containing subunit H constructs expressed from a pRS316 plasmid were affinity purified as above, also using a plasmidborne G subunit carrying an N-terminal FLAG tag. Human subunit H variants HsH1 and HsH2 were expressed in *E. coli* as N-terminal GST fusions. A detailed description of the ScV_1 and subunit H purifications can be found in the Appendix Supplementary Methods.

Crystallogenesis, data collection, phasing, and refinement

Crystals for the 7-Å dataset were obtained in a microfluidic plate (Microlytics High Throughput Plate) in 9.5% PEG 8000, 150 mM $(NH_4)_2SO_4$, 100 mM HEPES pH 7.5 and 12.5 mM $MgCl_2$ using 3 mg/ml of ScV_1. The needle-shaped crystals appeared after ~2 weeks and grew to maximum dimensions of 0.3 × 0.1 × 0.1 mm. Crystals for the 6.2–6.5 Å dataset were obtained using the hanging drop vapor diffusion setup at 10 mg/ml ScV_1 in 8.25% PEG 8000, 250 mM $(NH_4)_2SO_4$, 100 mM HEPES pH 7.5, and 50 mM $SrCl_2$. Since diffraction of the slightly better crystals (visible spots to 6.2 Å) was anisotropic, the dataset was submitted to the anisotropy server at UCLA (Strong *et al*, 2006) and elliptically truncated to 6.5, 6.2, and 6.7 Å as suggested by the server. Completeness of the dataset after truncation is shown in Appendix Table S1. The structure from the 7 Å dataset was solved by molecular replacement using the A_3B_3 complex of nucleotide-free EhV_1 (3vr5) (Arai *et al*, 2013). The resulting electron density map allowed modeling of the N- and C-terminal domains of subunit H (1ho8) (Sagermann *et al*, 2001) and the N- and C-terminal α-helices of subunit D (3vr5). Cycles of refinement, density modification, and NCS averaging allowed modeling of subunits E and G (4dl0) (Oot *et al*, 2012a). The refined model was then used to solve the structure of the 6.2–6.5 Å dataset. The resulting map allowed placement of the base of subunit D and subunit F (4rnd) (Balakrishna *et al*, 2015) and extension of the N-termini of peripheral stalks EG2 and EG3 (4dl0). For both structures, side chains were not modeled due to the limited resolution of the data. Details of the structure determination and refinement can be found in the Appendix Supplementary Methods. A stereo representation of the final electron density map is shown in Appendix Fig S2.

H subunit constructs and site-directed mutagenesis

A yeast strain deleted for the genes encoding subunits H (VMA13) and G (VMA10) (vma13Δ::KanMX, vma10Δ::Nat) (Diab *et al*, 2009) was transformed with a pRS315 plasmid containing N-terminally FLAG tagged G subunit and a pRS316 plasmid containing untagged human H isoforms (HsH1, HsH2), myc-tagged chimeric H subunit (H_{Chim}), helix truncated yeast H (H_{Loop}) as well as D410A (H_{D410A}) mutants. Transformants were selected on double dropout (SD −Ura, −Leu) medium and tested for complementation of the Vma^- phenotype by growth at pH 7.5 in the presence of 60 mM Ca^{2+}. A detailed description of the yeast and human subunit H constructs can be found in the Appendix Supplementary Methods.

ATPase activity assays and endogenous nucleotide content

ATPase activity of the purified ScV_1 sectors was measured in an ATP regenerating assay as described (Zhang *et al*, 2003; Diab *et al*, 2009). Endogenous nucleotide content of ScV_1 and $ScV_1\Delta H$ were measured using the ATP Bioluminescence Assay Kit CLSII (Roche) on a BioTek Synergy HT Luminometer. ATPase and nucleotide content measurements are described in detail in the Appendix Supplementary Methods.

Other methods

Figures and movies were generated in UCSF Chimera (Yang *et al*, 2012).

Accession codes

Protein Data Bank: Structure factors and atomic coordinates for the 7 and 6.2–6.5 Å resolution ScV_1 structures have been deposited with accession codes 5BW9 and 5D80, respectively.

Expanded View for this article is available online.

Acknowledgements

The authors would like to thank Dr. Masashi Ohira for his contributions to the initial phase of this project and Dr. Thomas Duncan for use of the Luminometer and technical assistance with nucleotide measurements. We thank the beamline staff at MacCHESS (Cornell University) and IMCA-CAT (Advanced Photon Source beamline 17-ID at Argonne National Labs) for beam time and help with data collection. Part of this work is based upon research conducted at the Cornell High Energy Synchrotron Source (CHESS), which is supported by the National Science Foundation and the National Institutes of Health/National Institute of General Medical Sciences under NSF award DMR-1332208, using the Macromolecular Diffraction at CHESS (MacCHESS) facility, which is supported by award GM-103485 from the National Institute of General Medical Sciences, National Institutes of Health. Financial support for this study was provided by the US National Institutes of Health grant GM058600 to S.W.

Author contributions

RAO and SW collected/processed the diffraction data, solved, and refined the structure and wrote the manuscript. RAO purified and optimized crystallization of V_1, made the H subunit mutant constructs, performed the ATPase and nucleotide assays. PMK generated the subunit G, subunit C deletion yeast strain used for ScV_1 purification, provided the $V_1\Delta H$ strain and the pRS316-mycVMA13 plasmid in which the H subunit mutations were constructed. EAB provided technical advice with data analysis and structure refinement.

Conflict of interest

The authors declare that they have no conflict of interest.

References

Arai S, Saijo S, Suzuki K, Mizutani K, Kakinuma Y, Ishizuka-Katsura Y, Ohsawa N, Terada T, Shirouzu M, Yokoyama S, Iwata S, Yamato I, Murata T (2013) Rotation mechanism of *Enterococcus hirae* V1-ATPase based on asymmetric crystal structures. *Nature* 493: 703 – 707

Arai S, Yamato I, Shiokawa A, Saijo S, Kakinuma Y, Ishizuka-Katsura Y, Toyama M, Terada T, Shirouzu M, Yokoyama S, Iwata S, Murata T (2009) Reconstitution in vitro of the catalytic portion (NtpA3-B3-D-G complex) of Enterococcus hirae V-type Na+-ATPase. *Biochem Biophys Res Commun* 390: 698 – 702

Balakrishna AM, Basak S, Manimekalai MS, Gruber G (2015) Crystal structure of subunits D and F in complex gives insight into energy transmission of the eukaryotic V-ATPase from *Saccharomyces cerevisiae*. *J Biol Chem* 290: 3183 – 3196

Benlekbir S, Bueler SA, Rubinstein JL (2012) Structure of the vacuolar-type ATPase from *Saccharomyces cerevisiae* at 11-A resolution. *Nat Struct Mol Biol* 19: 1356 – 1362

Bowman EJ, Bowman BJ (2005) V-ATPases as drug targets. *J Bioenerg Biomembr* 37: 431 – 435

Brown D, Smith PJ, Breton S (1997) Role of V-ATPase-rich cells in acidification of the male reproductive tract. *J Exp Biol* 200: 257 – 262

Couoh-Cardel S, Milgrom E, Wilkens S (2015) Affinity purification and structural features of the yeast vacuolar ATPase Vo membrane sector. *J Biol Chem* 290: 27959 – 27971

Diab H, Ohira M, Liu M, Cobb E, Kane PM (2009) Subunit interactions and requirements for inhibition of the yeast V1-ATPase. *J Biol Chem* 284: 13316 – 13325

Diakov TT, Kane PM (2010) Regulation of vacuolar proton-translocating ATPase activity and assembly by extracellular pH. *J Biol Chem* 285: 23771 – 23778

Fais S, De Milito A, You H, Qin W (2007) Targeting vacuolar H+-ATPases as a new strategy against cancer. *Cancer Res* 67: 10627 – 10630

Flannery AR, Stevens TH (2008) Functional characterization of the N-terminal domain of subunit H (Vma13p) of the yeast vacuolar ATPase. *J Biol Chem* 283: 29099 – 29108

Forgac M (2007) Vacuolar ATPases: rotary proton pumps in physiology and pathophysiology. *Nat Rev Mol Cell Biol* 8: 917 – 929

Futai M, Nakanishi-Matsui M, Okamoto H, Sekiya M, Nakamoto RK (2012) Rotational catalysis in proton pumping ATPases: from *E. coli* F-ATPase to mammalian V-ATPase. *Biochim Biophys Acta* 1817: 1711 – 1721

Graf R, Harvey WR, Wieczorek H (1996) Purification and properties of a cytosolic V1-ATPase. *J Biol Chem* 271: 20908 – 20913

Hildenbrand ZL, Molugu SK, Stock D, Bernal RA (2010) The C-H peripheral stalk base: a novel component in V1-ATPase assembly. *PLoS ONE* 5: e12588

Ho MN, Hirata R, Umemoto N, Ohya Y, Takatsuki A, Stevens TH, Anraku Y (1993) VMA13 encodes a 54-kDa vacuolar H(+)-ATPase subunit required for activity but not assembly of the enzyme complex in *Saccharomyces cerevisiae*. *J Biol Chem* 268: 18286 – 18292

Inoue H, Noumi T, Nagata M, Murakami H, Kanazawa H (1999) Targeted disruption of the gene encoding the proteolipid subunit of mouse vacuolar H(+)-ATPase leads to early embryonic lethality. *Biochim Biophys Acta* 1413: 130 – 138

Jefferies KC, Forgac M (2008) Subunit H of the vacuolar (H+) ATPase inhibits ATP hydrolysis by the free V1 domain by interaction with the rotary subunit F. *J Biol Chem* 283: 4512 – 4519

Kane PM (1995) Disassembly and reassembly of the yeast vacuolar H(+)-ATPase *in vivo*. *J Biol Chem* 270: 17025 – 17032

Karet FE, Finberg KE, Nelson RD, Nayir A, Mocan H, Sanjad SA, Rodriguez-Soriano J, Santos F, Cremers CW, Di Pietro A, Hoffbrand BI, Winiarski J, Bakkaloglu A, Ozen S, Dusunsel R, Goodyer P, Hulton SA, Wu DK, Skvorak AB, Morton CC *et al* (1999) Mutations in the gene encoding B1 subunit of H+-ATPase cause renal tubular acidosis with sensorineural deafness. *Nat Genet* 21: 84 – 90

Kartner N, Manolson MF (2014) Novel techniques in the development of osteoporosis drug therapy: the osteoclast ruffled-border vacuolar H(+)-ATPase as an emerging target. *Expert Opin Drug Discov* 9: 505 – 522

Kitagawa N, Mazon H, Heck AJ, Wilkens S (2008) Stoichiometry of the peripheral stalk subunits E and G of yeast V1-ATPase determined by mass spectrometry. *J Biol Chem* 283: 3329 – 3337

Liu M, Tarsio M, Charsky CM, Kane PM (2005) Structural and functional separation of the N- and C-terminal domains of the yeast V-ATPase subunit H. *J Biol Chem* 280: 36978 – 36985

Lu X, Yu H, Liu SH, Brodsky FM, Peterlin BM (1998) Interactions between HIV1 Nef and vacuolar ATPase facilitate the internalization of CD4. *Immunity* 8: 647 – 656

Muench SP, Trinick J, Harrison MA (2011) Structural divergence of the rotary ATPases. *Q Rev Biophys* 44: 311 – 356

Nagamatsu Y, Takeda K, Kuranaga T, Numoto N, Miki K (2013) Origin of asymmetry at the intersubunit interfaces of V1-ATPase from Thermus thermophilus. *J Mol Biol* 425: 2699 – 2708

Oot RA, Huang LS, Berry EA, Wilkens S (2012a) Crystal structure of the yeast vacuolar ATPase heterotrimeric EGC(head) peripheral stalk complex. *Structure* 20: 1881 – 1892

Oot RA, Wilkens S (2012b) Subunit interactions at the V1-Vo interface in yeast vacuolar ATPase. *J Biol Chem* 287: 13396 – 13406

Parra KJ, Kane PM (1996) Wild-type and mutant vacuolar membranes support pH-dependent reassembly of the yeast vacuolar H+-ATPase *in vitro*. *J Biol Chem* 271: 19592 – 19598

Parra KJ, Kane PM (1998) Reversible association between the V1 and V0 domains of yeast vacuolar H+-ATPase is an unconventional glucose-induced effect. *Mol Cell Biol* 18: 7064 – 7074

Parra KJ, Keenan KL, Kane PM (2000) The H subunit (Vma13p) of the yeast V-ATPase inhibits the ATPase activity of cytosolic V1 complexes. *J Biol Chem* 275: 21761 – 21767

Powell B, Graham LA, Stevens TH (2000) Molecular characterization of the yeast vacuolar H+-ATPase proton pore. *J Biol Chem* 275: 23654 – 23660

Sagermann M, Stevens TH, Matthews BW (2001) Crystal structure of the regulatory subunit H of the V-type ATPase of *Saccharomyces cerevisiae*. *Proc Natl Acad Sci USA* 98: 7134 – 7139

Sautin YY, Lu M, Gaugler A, Zhang L, Gluck SL (2005) Phosphatidylinositol 3-kinase-mediated effects of glucose on vacuolar H+-ATPase assembly, translocation, and acidification of intracellular compartments in renal epithelial cells. *Mol Cell Biol* 25: 575 – 589

Sennoune SR, Bakunts K, Martinez GM, Chua-Tuan JL, Kebir Y, Attaya MN, Martinez-Zaguilan R (2004) Vacuolar H+-ATPase in human breast cancer cells with distinct metastatic potential: distribution and functional activity. *Am J Physiol Cell Physiol* 286: C1443 – C1452

Seol JH, Shevchenko A, Shevchenko A, Deshaies RJ (2001) Skp1 forms multiple protein complexes, including RAVE, a regulator of V-ATPase assembly. *Nat Cell Biol* 3: 384 – 391

Smardon AM, Tarsio M, Kane PM (2002) The RAVE complex is essential for stable assembly of the yeast V-ATPase. *J Biol Chem* 277: 13831 – 13839

Smardon AM, Nasab ND, Tarsio M, Diakov TT, Kane PM (2015) Molecular interactions and cellular itinerary of the yeast RAVE (regulator of the H+-ATPase of vacuolar and endosomal membranes) complex. *J Biol Chem* 290: 27511 – 27523

Smith AN, Skaug J, Choate KA, Nayir A, Bakkaloglu A, Ozen S, Hulton SA, Sanjad SA, Al-Sabban EA, Lifton RP, Scherer SW, Karet FE (2000) Mutations in ATP6N1B, encoding a new kidney vacuolar proton pump 116-kD subunit, cause recessive distal renal tubular acidosis with preserved hearing. *Nat Genet* 26: 71 – 75

Stransky LA, Forgac M (2015) Amino acid availability modulates vacuolar H+-ATPase assembly. *J Biol Chem* 290: 27360 – 27369

Strong M, Sawaya MR, Wang S, Phillips M, Cascio D, Eisenberg D (2006) Toward the structural genomics of complexes: crystal structure of a PE/PPE protein complex from *Mycobacterium tuberculosis*. *Proc Natl Acad Sci USA* 103: 8060 – 8065

Sumner JP, Dow JA, Earley FG, Klein U, Jager D, Wieczorek H (1995) Regulation of plasma membrane V-ATPase activity by dissociation of peripheral subunits. *J Biol Chem* 270: 5649 – 5653

Sun-Wada GH, Toyomura T, Murata Y, Yamamoto A, Futai M, Wada Y (2006) The a3 isoform of V-ATPase regulates insulin secretion from pancreatic beta-cells. *J Cell Sci* 119: 4531 – 4540

Thudium CS, Jensen VK, Karsdal MA, Henriksen K (2012) Disruption of the V-ATPase functionality as a way to uncouple bone formation and resorption – a novel target for treatment of osteoporosis. *Curr Protein Pept Sci* 13: 141 – 151

Trombetta ES, Ebersold M, Garrett W, Pypaert M, Mellman I (2003) Activation of lysosomal function during dendritic cell maturation. *Science* 299: 1400 – 1403

Voss M, Vitavska O, Walz B, Wieczorek H, Baumann O (2007) Stimulus-induced phosphorylation of vacuolar H(+)-ATPase by protein kinase A. *J Biol Chem* 282: 33735 – 33742

Wilkens S, Inoue T, Forgac M (2004) Three-dimensional structure of the vacuolar ATPase. Localization of subunit H by difference imaging and chemical cross-linking. *J Biol Chem* 279: 41942 – 41949

Williamson WR, Hiesinger PR (2010) On the role of v-ATPase V0a1-dependent degradation in Alzheimer disease. *Commun Integr Biol* 3: 604 – 607

Xu Y, Parmar A, Roux E, Balbis A, Dumas V, Chevalier S, Posner BI (2012) Epidermal growth factor-induced vacuolar (H+)-atpase assembly: a role in signaling via mTORC1 activation. *J Biol Chem* 287: 26409 – 26422

Yang Z, Lasker K, Schneidman-Duhovny D, Webb B, Huang CC, Pettersen EF, Goddard TD, Meng EC, Sali A, Ferrin TE (2012) UCSF Chimera, MODELLER, and IMP: an integrated modeling system. *J Struct Biol* 179: 269 – 278

Zhang J, Feng Y, Forgac M (1994) Proton conduction and bafilomycin binding by the V0 domain of the coated vesicle V-ATPase. *J Biol Chem* 269: 23518 – 23523

Zhang Z, Charsky C, Kane PM, Wilkens S (2003) Yeast V1-ATPase: affinity purification and structural features by electron microscopy. *J Biol Chem* 278: 47299 – 47306

Zhang Z, Zheng Y, Mazon H, Milgrom E, Kitagawa N, Kish-Trier E, Heck AJ, Kane PM, Wilkens S (2008) Structure of the yeast vacuolar ATPase. *J Biol Chem* 283: 35983 – 35995

Zhao J, Benlekbir S, Rubinstein JL (2015) Electron cryomicroscopy observation of rotational states in a eukaryotic V-ATPase. *Nature* 521: 241 – 245

